Neutron studies of gauge field and charge in Ih heavy-water ice

D. J. P. Morris, K. Siemensmeyer, J.-U. Hoffmann, B. Klemke, I. Glavatskyi, K. Seiffert, D. A. Tennant, S. V. Isakov, S. L. Sondhi, and R. Moessner

Phys. Rev. B **99**, 174111 — Published 20 May 2019

DOI: 10.1103/PhysRevB.99.174111

Neutron studies of gauge field and charge in Ih heavy-water ice

D.J.P. Morris,[1] K. Siemensmeyer,[2] J.-U. Hoffmann,[2] B. Klemke,[2] I. Glavatskyi,[3]
K. Seiffert,[4] D.A. Tennant,[5] S.V. Isakov,[6] S.L. Sondhi,[7] and R. Moessner[8]

[1]*Department of Physics, Xavier University, 3800 Victory Parkway, Cincinnati, OH 45207, U.S.A.**
[2]*Helmholtz-Zentrum Berlin, Hahn-Meitner Platz 1, Berlin, Germany.*
[3]*Scienion AG, Volmerstr. 7b, D-12489 Berlin, Germany.*
[4]*Technische Universität Berlin, Pascalstr. 8-9, D-10587, Germany.*
[5]*Oak Ridge National Laboratory, P.O. Box 2008 MS-6477, Oak Ridge, TN 37831, U.S.A.*
[6]*Google Inc., Brandschenkestrasse 110, 8002 Zurich, Switzerland.*
[7]*Department of Physics, Princeton University, Washington Road, Princeton, NJ 08544, U.S.A.*
[8]*Max-Planck-Institut für Physik komplexer Systeme,*
Nothnitzer Strasse 38, D-01187 Dresden, Germany.

(Dated: May 2, 2019)

The distinctive character of water ice results from the partially disordered combination of covalent and hydrogen bonds in the network of hydrogen and oxygen atoms. The non-trivial hydrogen correlations we report in diffuse neutron scattering are analytically fit via a description of this state as a topological system exhibiting an emergent gauge field. This allows for the density of correlation terminating point-defects to be determined as one defect per 500 oxygen sites at 30 K. Application of an analytical model of ice paves the way towards a detailed understanding of this ubiquitous solid.

61.05.F-, 31.70.Ks, 61.72.Ji:

I. INTRODUCTION

Water ice (H_2O) is a unique solid whose structure and dynamics continue to excite interest. The special connectivity of the ${}_{H}O_{H}$ polar molecules through the making and breaking of hydrogen bonds forms a dynamic network which can reconfigure to transport charge [1] while being of importance in a truly interdisciplinary range of fields from food science to biology [2]. In its common form, ice is made up of H_2O molecules within a hexagonal-close-packed unit cell (Fig. 1a), referred to as the Ih phase well known in everyday live. The oxygen atoms form a regular lattice, and each oxygen is surrounded by four hydrogen ions (protons, H^+), each located on a line connecting the four nearest neighbor oxygen sites (Fig. 1b). The hydrogens are displaced from the midpoints between two oxygens and each oxygen has two close hydrogens, keeping the H_2O molecular character. These structural constraints are encoded by the Bernal-Fowler ice rules [3], implying the residual ground-state entropy [4] of $Rln\frac{3}{2}$ and the commonly accepted picture of hydrogen disorder: in the ground-state, H_2O molecules form a quasi-degenerate correlated network where the orientation of one molecule affects the orientation of adjacent molecules, which in turn affects the orientation of further molecules, propagating throughout the crystal. Previous diffuse elastic X-ray and neutron scattering studies of ice confirmed the ice rules using simulations where molecules are orientated along random walks restricted by the ice rules (Refs. 5–7) but lacked a description of the mechanism that led to the structure.

* morrisd3@xavier.edu

Work to combine ideas from topology and field theory along with a simple mapping of hydrogen displacement vectors onto pseudospins (Refs. 8–14) has culminated in the development of a theoretical approach by Isakov, et al. [15] and Benton, et al. [16]. We present a diffuse neutron scattering experiment that tests this topoligical description of the structure of water ice at 30 K. While scattering intensity of Bragg peaks reveals the long-range average occupation of crystallographic sites, diffuse scattering probes structural correlations of materials over a large spatial range from small displacement to long-range correlations. Diffuse scattering data covering a 3D volume of reciprocal space provides a large dataset to robustly test the theoretical predictions on the nano- to meso-scale structure.

The key idea of the topological order approach (Refs. 15 and 16) is that the displacement vector from the oxygen bond midpoint to the occupied hydrogen site (Fig. 1b) is modelled as an Ising pseudospin, $\vec{s}_i$ (Ref. 12). The locations of the occupied hydrogen sites are given by $\vec{r}_{i\alpha} = \vec{r}^{\,0}_{i\alpha} + d\vec{s}_{i\alpha}$ where $\vec{r}^{\,0}_{i\alpha}$ is the location of the midpoint between nearest neighbor oxygen-oxygen, $d = 0.134\mathrm{R_{OO}}$ is the length of the hydrogen displacement away from the center of the bond and $\mathrm{R_{OO}}$ is the neighboring oxygen-oxygen distance, 2.76 Å. The pseudospins $\vec{s}_{i\alpha}$=±1 indicate a nearby or far-away hydrogen for the hydrogen ion labeled α in the i^{th} unit cell and should not be confused with any quantum mechanical spin in the system. Infact, the pseudospin is a manifestation of an emergent gauge-field, labelled $\vec{B}$, aligned with the pseudospins (Fig. 1c, Ref. 8). In a ground state, the total number of vectors pointing into each oxygen is equal to the number pointing out therefore the ice-rules imply the averaged field to be divergence-free, $\nabla \cdot \vec{B} = 0$, as in conventional

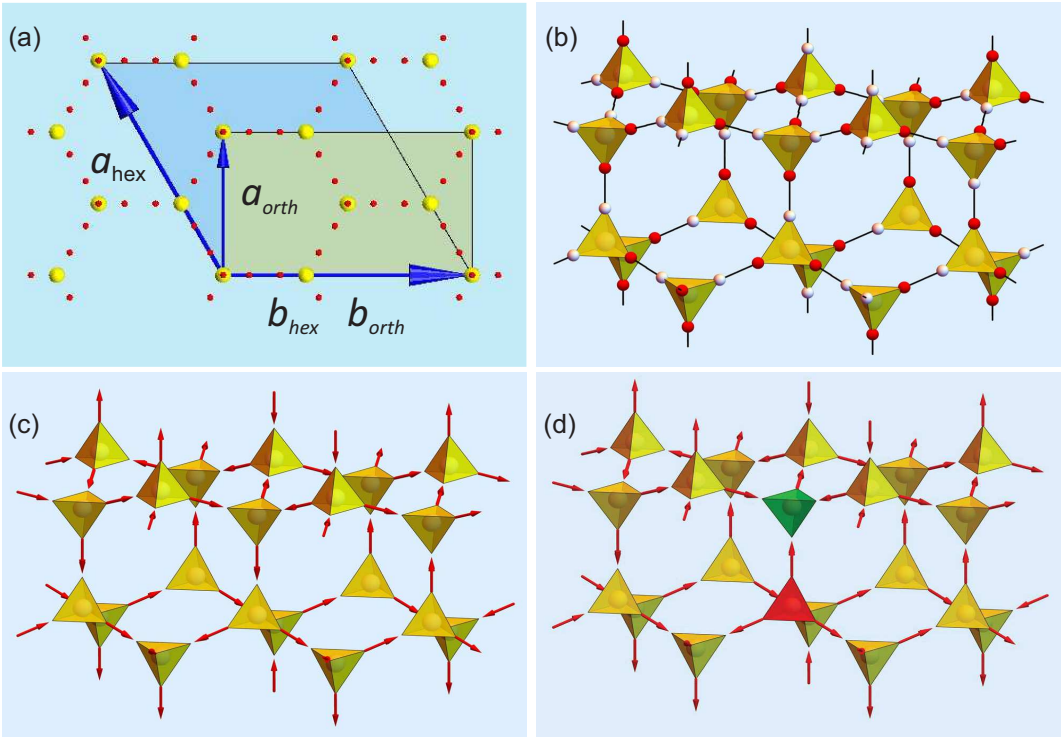

FIG. 1. The Coulomb liquid structure of water ice. a) The Ih phase of water ice is made up of hexagonal unit cells ($\vec{a}_{hex}, \vec{b}_{hex}$) although an equally justifiable unit cell is the smaller orthogonal unit cell used in this study ($\vec{a}_{orth}, \vec{b}_{orth}$), shown here with yellow oxygen and red hydrogen sites. b) The water molecules in the common form of ice (Ih) are arranged as connected tetrahedra obeying the ice rules. The oxygen sits at the center of the tetrahedron, surrounded by four protons which can occupy one of two possible sites shown in red (vacant) and white (occupied) between any pair of neighboring oxygens. (c) The displacement of the occupied hydrogen site away from the O-O midpoint is modeled as a pseudospin [15]. (d) Point defects terminate the hydrogen correlations and break the ice rules locally, e.g. net plus (H_3O^+, green) and minus charges (OH^-, pink) can form, separate via pseudospin flips, and carry electric current.

magnetostatics. A review of systems exhibiting emergent electromagnetic states is given in Ref. 17 and one on topology and (spin) ice physics in Ref. 18.

II. EXPERIMENT

A. Sample Preparation

Heavy water ice (D_2O) samples were used that contained the deuterium isotope, instead of hydrogen, as it provides less incoherent background in neutron scattering [19]. High quality single-crystals of D_2O were grown with a modified Bridgeman technique based on work by Ohtomo [20] where a temperature gradient slowly moves along a sample growth cell containing liquid D_2O.

The crystal growth apparatus has been constructed from a cold liquid bath (23% ethylene glycol:water solution) cooled by a Julbo refrigeration circulator to temperatures below the freezing point of D_2O, $<4\,^\circ$C, into which the sample growth cell could be immersed in a controlled way by a stepper motor (fig. 2) and the entire assembly was housed in a cold room at the Helmholtz-Zentrum Berlin (HZB) which was kept between 6-10 °C. The single crystal is selected from the polycrystalline ice, formed at the bottom of the growth cell, by continuous change in direction due to the lower part of the sample growth cell having a spiral form with a narrow sealed section at the lower end and a constriction at the upper end of the spiral. Ideally one crystallite emerges from the spiral and continues to grow in a long straight silicone-rubber tube of 10 mm inner-diameter. The heating gradient was enforced by a circular heater placed around the growth cell about 3 cm above the ethelyne glycol solution. Before growth, the starting D_2O in the cell was degassed by vacuum pumping and was sealed to prevent air contamination during growth leading to a vapour pressure of approximately 30 mbar during growth. This growth method produced approximately 12 cm long crystals over one week. The crystal was removed from the cell by cutting the rubber along its length, and then cleaved perpendicular to its length into three pieces, one of which was used for the experiment. Crystal quality was tested using birefringence in the cold room or, when weather allowed, outside in the cold Berlin winter. The birefringence revealed the samples were composed of two twinned crystallites forming half-cylinders along the entire length

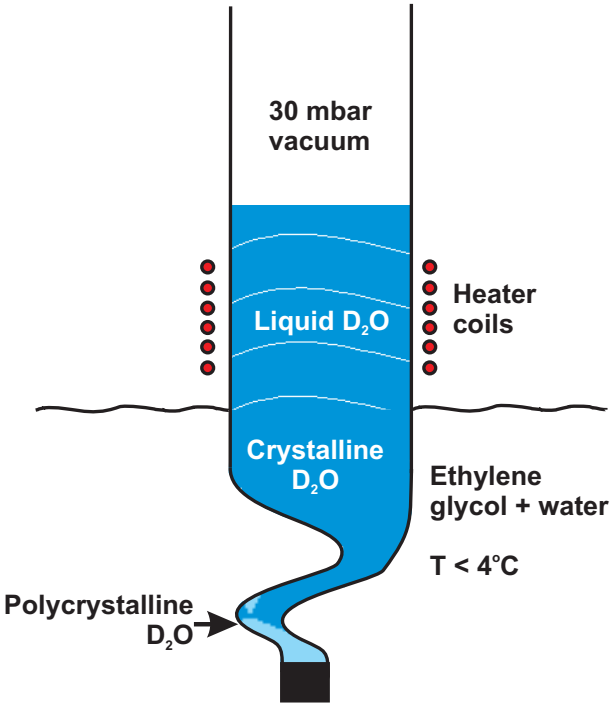

FIG. 2. (Color online) Single crystal growth cell based on work by Ohtomo [20]. Rubber tube connected to a plastic spiral filled with D_2O is passed between heater coils and then lowered into cooled ethylene glycol solution. Polycrystalline ice forms in the spiral and directional changes select a single crystal with propagates into the main sample cell.

of the sample. One twin, a half-cylinder of 1 cm diameter and 2 cm length, was cleaved and crystallinity was tested using X-ray Laue diffraction at a number of spots on all sides of the crystal during which time the samples were orientated for the neutron measurements.

B. Neutron Scattering

The structural correlations were measured on the E2 diffractometer at the BER-II reactor, Helmholtz-Zentrum Berlin, Germany [21] which uses a flat-cone geometry and position sensitive area detectors allow the measurement of the scattering intensity throughout volumes in 3D reciprocal space. Neutrons with a wavelength of 1.2 Åwere obtained using a [1,1,1] Ge monochromator with a 30' collimation. Data were collected by rotating the sample axis in steps of 1°, counting at each step for 1 minute. The sample was oriented with the b-c plane in the horizontal scattering plane with data perpendicular to this plane being measured by synchronously tilting detector bank and sample out of the scattering plane. Data were collected at 30 K using three different detector inclination angles between 0° and 30°. For the analysis, the data were transformed from angular space into three-dimensional reciprocal space using the orthorhombic unit cell (Fig 1a) for Ih ice [22]. Lattice constants were checked with E2 and E10 diffractometer at HZB and were found to be a_{E2}=4.30 Å, b_{E2}=7.71 Å, c_{E2}=7.27 Åon E2 agreeing with literature [22] within the E2 instrument omega resolution of 1°, and a_{E10}=4.51 Å, b_{E10}=7.82 Åon E10 with less than 1% uncertainty. A closed cycle refrigerator (CCR) kept the sample cold during measurmenets on E2 and E10 and the sample was transferred into the CCR under cold N_2 atmosphere. To reduce background scattering the sample mount was covered with Cadmium and the CCR was operated without radiation shields. The lowest achievable temperature, and the temperature used in the neutron experiment, was 30 K.

III. DATA AND ANALYSIS

A. 3D fit to experimental data

The diffuse scattering between Bragg peaks shows broad features which reflect the hydrogen correlations. We analyse the 3D volume of neutron scattering data using a large-N approach [15]. Crucially, it captures both the short range hydrogen correlations, as well as the long range distance decay, in a unified analytical way. The actual analysis involves essentially standard diagonalization of the interaction matrix by the bonds of the oxygen network of ice, which is technically straightforward to carry out. Its nonstandard character – compared to conventional magnetic systems – lie in the nature of the solution thus obtained: the system avoids long-range order down to the lowest temperatures, and instead exhibits an extensive space of residual low-energy degrees of freedom. It is these which encode the emergent gauge structure.

The calculated intensity, $I(Q)$, used in the fit is given by:

$$I(Q) = I_0 \cdot G(Q,d,T') \cdot e^{(-BQ^2)} + a_0 + a_1|Q| + a_2|Q|^2 \quad (1)$$

Here I_0 is the incident neutron intensity per detector pixel in each 0.05 x 0.05 x 0.05 r.l.u. Q-space volume element; $G(Q,d,T\prime)$ is the theoretical structure factor where d is the proton displacement away from the O-O bond

TABLE I. Theoretical fit parameters. The best fit parameters from a simultaneous fit of the 3D experimental data at 30 K. Where "arb. units" represents arbitrary units, "arb. units Å" and "arb. units Å^2" refer to the same arbitrary units multiplied by Angstroms and Angstroms-squared respectively.

	Fit parameter	Standard error
a_0 (arb. units)	0.2699	0.0011
a_1 (arb. units Å)	0.064	0.002
a_2 (arb. units Å^2)	-0.066	0.002
T' (J)	0.57	0.08
I_0 (arb. units)	0.68	0.02
B (Å^2)	0.161	0.08

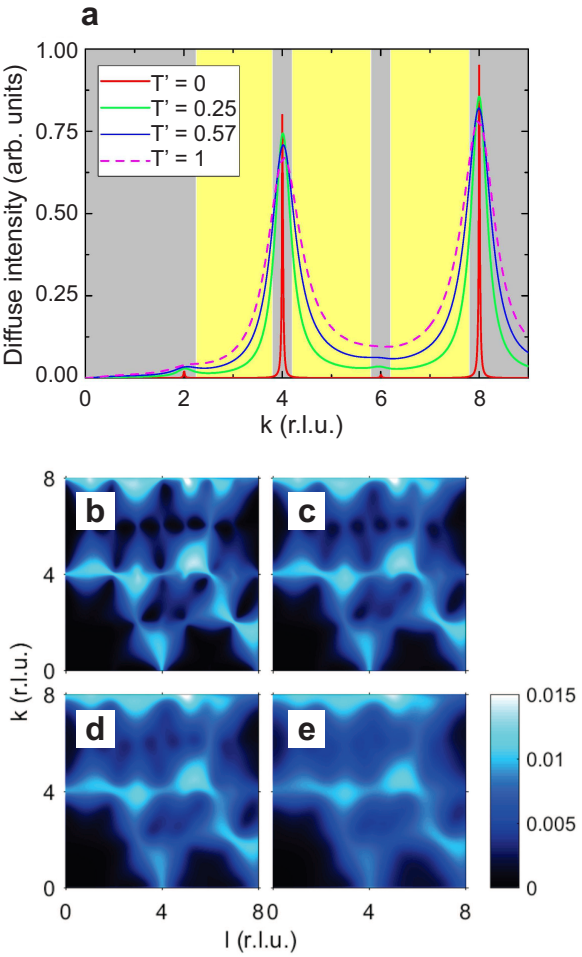

FIG. 3. (Color online) Variation of theoretical diffuse scattering with respect to theoretical effective temperature, T. (a) The dependence of the theoretical diffuse scattering along (0,k,0) from hydrogen atoms on the value of the theoretical parameter T, from the large-N theory with L=16 (L^3 is the number of units cells). At finite T, the diffuse signal in the wings of the pinch points at $\vec{Q}$ = (0,4,0) and (0,8,0) shows very distinct behaviour as a function of Q. The light grey regions (yellow online) represent the Q-regions included in the fit to the experimental data showing a strong dependence on the calculated scattering with T. Calculated neutron scattering intensity in the (0,k, l) plane are shown for (b) $T' = 0.13J$, (c) $0.54J$, (d) $1.00J$, and (e) $2.00J$ revealing the dependence on T' of the diffuse scattering away from the pinch points. Therefore, a reliable value for T can be obtained from the fit without including pinch points and areas around oxygen Bragg peaks (dark grey regions in panel a).

midpoint and hence it is the length of the hydrogen displacement vector ($d = 0.134\,\mathrm{R_{OO}}$) [15]; the Debye-Waller factor ($e^{(-BQ^2)}$) accounts for the reduction in intensity due to atomic vibration; the remaining three terms account for the asymmetric background. The momentum transfer, Q, is the magnitude of the reciprocal lattice vector with coordinates (h, k, l). The model contains only one free parameter resembling temperature in the effective interaction matrix (see Ref. 15), T', in units of the interaction strength, J. The fit parameter T' characterises the energy scale of the gauge theory, J, at finite temperature (Fig. 3) and is related to the energy scale for the first excited state; i.e. T' sets the energy of the creation of ionic defect pairs in ice, H_3O^+, OH^- (Fig. 1d) which are the analogue to a monopole excitation in electromagnetism. The defect-defect correlation length, ξ, will increase proportionally with $e^{(+E/3k_BT')}$ (see fig. 3), where E is the defect creation energy. Altogether, within the large-N model the constants d and T' fully describe the proton structure and a significant amount of the dynamics of ice within this gauge theory. The other parameters used in the fit are related to the experimental set up. The experimental scattering data contains sharp Bragg peaks along with air scattering surrounding the intense Bragg peaks, neither of which are informative about the hydrogen correlations so the fit function does not take those artifacts into account. Therefore, regions of Q-space containing such scattering were excluded from the fit (Figs. 4a and 4c). The fit is quite robust against the method of excluding such data points with the effective interaction temperature always between $T' = 0.54J$ to $0.6J$ (Fig. 3), with the best fit parameters given in Table I. The resulting diffuse neutron scattering data and calculation using the fit parameters are shown in figure 4 showing good agreement; the theory analytically fits the 3D diffuse scattering data from ice Ih.

B. Defect-Defect Correlation Lengths, Pinch Points, and Defect Density

This analytic approach provides a new method of probing ice properties that so far have not been accessible experimentally, namely the determination of the defect density that is highly relevant e.g. for electrical transport properties of ice. At sufficiently low temperatures, the ice rules are essentially almost perfectly obeyed modulo the presence of dilute defects. The experimental hydrogen correlations terminate at dilute point-defects in the hydrogen structure either ionic defects (OH^-, H_3O^+), Bjerrum defects (either zero or two hydrogens between nearest neighbor oxygen referred to as L- and D-defects respectively, Ref. 23) or defects in the molecular structure (e.g. impurity ions, voids). In the ice literature many properties are explained by the presence and mobility of such electrically charged defects [24, 28]. Natural ice is usually impure and in part for this reason a lot of studies have focused on doped ice, in particular for electrical transport properties. Within the ice literature a separation of the ionic and Bjerrum defect signal from impurities is therefore difficult.

In the diffuse scattering from matter described by gauge fields (e.g. water ice, spin ice) correlations are evident as broad features which narrow down into a pinch-point, resembling a bowtie, at specific locations in reciprocal space [15, 17]. At finite temperature, the field

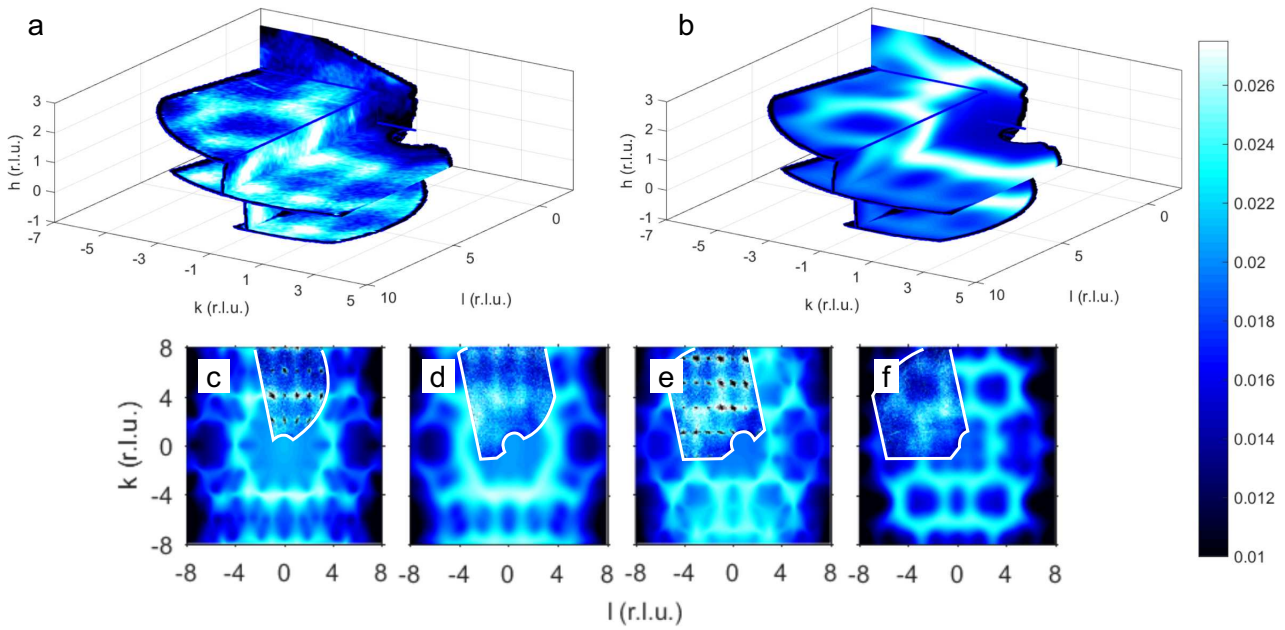

FIG. 4. Dipolar correlations in ice at 30 K. (a) Three-dimensional representation of the experimental neutron scattering data on non-integer indexed reciprocal space planes reveal diffuse textured features that come from the non-trivial hydrogen correlations. The data shown here are the $(h, k, -0.45)$, $(h, -0.45, l)$, $(h, -1.45, l)$, $(-0.45, k, l)$, $(0.55, k, l)$ and $(1.55, k, l)$ planes in reciprocal space. (b) The scattering calculated with theory of Isakov et al. (Ref. 15) using the parameters determined from the 3D fit to experimental data (Equation 1, Table I). Further agreement between experiment and theory is shown on the (c) (0,k,l), (d) (0.5,k,l), (e) (1.5,k,l), and (f) (2.0,k,l) reciprocal lattice planes. The experimental neutron scattering data is shown inside the white lines, with black regions of the experimental data showing Bragg peaks and air scattering not included in the fit.

lines, and therefore the hydrogen correlations in water ice terminate at defects separated on average by the defect-defect correlation length, which experimentally is the inverse of the pinch-point width. In an ice crystal without defects, i.e. a crystal with only closed field lines, these pinch points would be perfectly sharp and as defects are created, e.g. as temperature increases, the pinch-points would be expected to broaden. The low-intensity pinch points and the intense Bragg peaks from the average structure, unfortunately, appear at the same positions in Qspace in the experimental data and in practice a reliable separation of these intensities at the pinch-point location is impossible. Since the experimental hydrogen correlations are quantitatively described by the theoretical fit to the experimental data, detail about the pinch-points widths are nonetheless accessible in the neutron scattering intensity calculated using the parameters used to fit the experimental data (Equation 1, Table I). In order to determine orthogonal correlation lengths, the (4,0,0), (0,4,0) and (0,0,4) pinch-points in the theoretical data are fit with a Lorentzian function and an asymmetric background along the h, k, and l reciprocal space directions respectively (Fig. 5a-c) using:

$$I(q) = \frac{I_0^L \zeta^2}{\zeta^2 + (Q - Q_{hkl})^2} + I_{asym} \qquad (2)$$

The first term is the Lorentzian lineshape, where I_0^L is the intensity at (h, k, l); ζ is the full-width-half-maximum of the Lorentzian at (h, k, l) measured in reciprocal lattice units and therefore related to the defect-defect correlation length, ξ, by $\zeta = 1/\xi$; Q is the magnitude of the reciprocal lattice vector; Q_{hkl} is the magnitude of the reciprocal lattice vector at the position of the (h, k, l) pinch point. The second term accounts for a low-intensity asymmetric background (Equation 3) with the assymetry being needed to fit the wings of the theoretical data although with little impact on the Lorentzian width due to the small assymetry.

$$I_{asym}(q) = \frac{I_{b0}}{1 + e^{\frac{\pm Q \mp Q_{b0}}{\sigma}}} + I_{bc} \qquad (3)$$

Where I_{b0} is the intensity at the center of the smoothed step function (second term) which is centered on Q_{b0}; the $\pm$ and $\mp$ controls whether the background has higher intensity at low-Q or high-Q; σ is the width of the step function; and I_{bc} is a constant background term. Other background functions, e.g. constant background and linear background, were used but did not fit the wings of the data well. The fit parameters are given in table II; the three orthogonal defect-defect correlation lengths are approximately 9 R_{OO} resulting in a defect density of one defect per 500 sites.

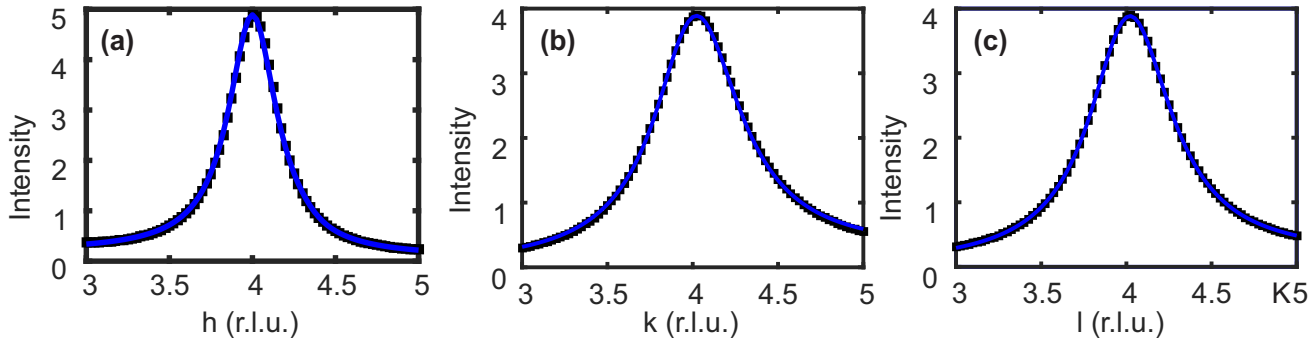

FIG. 5. (Color online) Defect density at 30 K. To determine the defect correlation lengths the pinch points at the (a) (4,0,0), (b) (0,4,0), and (c) (0,0,4) positions in reciprocal space in the theoretical data (black squares) were fitted using an asymmetric background and Lorentzian lineshapes (line).

TABLE II. Fit parameters of the (4,0,0), (0,4,0) and (0,0,4) pinch points in the large-N theoretical fit to the experimental data (Figs. 5e-5g). Where au is arbitrary units.

	ζ (r.l.u.)	ξ	I_{bc} (au)	I_{b0} (au)	σ (r.l.u.)	q_{b0} (r.l.u.)
(h,0,0)	0.1766	$5.663a = 25.5$ Å	7.6339	12.04	0.0464	4.35
(0,k,0)	0.3138	$3.186b = 24.9$Å	2.7x10^{-4}	25.23	0.0574	3.855
(0,0,l)	0.2985	$3.351c = 24.7$Å	2.7x10^{-4}	16.76	0.057	3.85

IV. DISCUSSION AND CONCLUSION

The experimental and theoretical methods shown here are promising tools to get more insight into the physics of ice. In principle the structure factor of the different defects could be used to distinguish between ionic and Bjerrum defects, but the Q-space range here and current data statistics precludes such an identification. Nevertheless, the technique reported here allows for a reliable determination of the density of the *total* number of defects. It is of interest to note that within the model, hopping of a hydrogen from one site along the OH-O bond to another site is described as reversal of the emergent field between neighboring oxygen-oxygen pair resulting in the flipping of an individual pseudospin creating a pair of emergent gauge charges. As the pseudospins also correlated with electric dipole moments on bonds (note that the molecular electric dipole moment would be the sum of the pseudospins coming into a particular oxygen), the resulting excitations in the theory also carry conventional electric charge and can be thought of (roughly) as plus (H_3O^+) and minus (OH^-) defects (Fig. 1c). The ionic defects, once created, are mobile through the reversal of neighboring pseudospins (i.e. neighboring protons moving between occupied and vacant sites) leading to molecular rotation along the path travelled by the ionic defect, retaining some of the structural mutability of the liquid phase and accounting, in part, for ices electrical conductivity [1, 26, 27]. It is important to note that the flipping of pseudospins to account for electrical conductivity is not in the quantum tunneling regime as predicted by Benton et al. [16] which occurs at much lower temperatures than were probed in this study.

The correlation length estimate here reveal an average defect density of one defect per 500 oxygen sites, corresponding to 1.2x10^{21} mol^{-1} in our sample at 30 K. That may be compared to previous high-temperature work where *higher* concentration would be expected: Gränicher reported that the defect densities at 263 K are 1.6x10^{12} mol^{-1} for ionic defects and 1.1x10^{17} mol^{-1} for Bjerrum defects [28]. Khamzin [29], when using a model of electrical relaxation due to ion hopping [30], shows that Gränicher's defect densities are not sufficient to account for the experimentally observed dielectric strengths at 200 K and 250 K [25]. Indeed, a defect density of 5.9x10^{22} mol^{-1}, approximately 50 times the density we found in our sample at 30 K, would be needed at 200 K and 250 K to account for the dielectric strengths. Further temperature dependent measurements of the defect density, such as ours, and of the dielectric constant would be instructive and shed more light to ths problem, but they are beyond the scope of the present study.

In summary, using neutron diffraction we show that the highly degenerate low-temperature structure of ice Ih is described by an analytical theory mapping ice-rule constrained hydrogen displacements onto an emergent electromagnetic field with U(1) symmetry. The hydrogen correlations follow its field lines and the field, mostly divergence-free, locally contains dilute point defects in the hydrogen correlations corresponding to weakly-interacting gauge charges. These charges terminate the field-lines and therefore degrade the hydrogen correlations. The success of the theory in fitting ice data is of general importance as it provides another tool in the analysis of diffuse scattering data

which probes the nano- and mesoscale disorder which in many functional materials underpins their sensitivity to external stimuli [31]. The usefulness of this technique is exemplified by the determination of the density of intrinsic point-defects which play an important role in the response of ice Ih to stimuli such as applied fields, with these defects being found to be present at one defect per 500 sites at 30 K in our sample. Whether cooperative effects of these point defects become more important to structural correlations or dynamics - e.g. as their density and quantum coherence varies with temperature - is an intriguing question which now is open to investigation.

ACKNOWLEDGMENTS

We wish to thank Thomas Hau, Andreas Hoser and Klaus Kiefer (HZB) for assistance on the experiment; Bella Lake and Eugen Weschke (HZB) for manuscript proof-reading; Owen Benton (OIST), Ivan A. Ryzhkin (ISSP) and D.T.W. Buckingham (MSU) for scientific discussions. We acknowledge financial support provided by the Helmholtz Association of German Research Centers as well as Deutsche Forschungsgemeinschaft under grants SFB 1143 and EXC 2147 ct.qmat. The research by DAT was sponsored by the Laboratory Directed Research and Development Program (LDRD) of Oak Ridge National Laboratory, managed by UT-Battelle, LLC, for the U.S. Department of Energy (Project ID 9566). Datasets containing neutron diffraction data and theoretical calculated data are available in reference [32].

[1] L. Onsager, *Nobel Lectures, Chemistry 1963-1970* (Elsevier Publishing Company, Amsterdam, 1972) Chap. Lars Onsager - Nobel Lecture: The motion of ions: principles and concepts.
[2] P. V. Hobbs, *Ice Physics* (Oxford University Press, 1974).
[3] J. D. Bernal and R. H. Fowler, J. Chem. Phys. **1**, 515 (1933).
[4] L. Pauling, J. Am. Chem. Soc. **57**, 2680 (1935).
[5] J. Schneider and C. Zeyen, J. Phys. C: Solid St. Phys. **13**, 4121 (1980).
[6] V. M. Nield, J. C. Li, D. K. Ross, and R. W. Whitworth, Phys. Scripta **T57**, 179 (1995).
[7] B. Wehinger, D. Chernyshov, M. Krisch, S. Bulat, V. Ezhov, and A. Bosak, J. Phys.: Condens. Matter **26**, 265401 (2014).
[8] J. Villain, Solid State Chem. **10**, 967 (1972).
[9] J. F. Nagle, Chem. Phys. **43**, 317 (1979).
[10] R. Youngblood, J. D. Axe, and B. M. McCoy, Phys. Rev. B **21**, 5212 (1980).
[11] R. W. Youngblood and J. D. Axe, Phys. Rev. B **23**, 232 (1981).
[12] I. Ryzhkin, Solid State Comm. **52**, 49 (1984).
[13] I. A. Ryzhkin, J. Exp. Theo. Phys. **88**, 1208 (1999).
[14] A. H. Castro Neto, P. Pujol, and E. Fradkin, Phys. Rev. B **74**, 024302 (2006).
[15] S. V. Isakov, R. Moessner, S. L. Sondhi, and D. A. Tennant, Phys. Rev. B **91**, 245152 (2015).
[16] O. Benton, O. Sikora, and N. Shannon, Phys. Rev. B **93**, 125143 (2016).
[17] C. L. Henley, Annu. Rev. Condens. Matter Phys. **1**, 179 (2010).
[18] C. Castelnovo, R. Moessner, and S. L. Sondhi, Annu. Rev. Condens. Matter Phys. **3**, 35 (2012).
[19] V. F. Sears, Neutron News **3**, 26 (1992).
[20] M. Ohtomo, S. Ahmad, and R. W. Whitworth, J. de Phys. **48**, C1 (1987).
[21] J.-U. Hoffmann and M. Reehuis, J. Large Scale Research Facilities **4**, A129 (2018).
[22] J. A. Hayward and J. R. Reimers, J. Chem. Phys. **106**, 1518 (1997).
[23] N. Bjerrum, Science **115**, 385 (1952).
[24] H. Engelhardt, B. Bullemer, and N. Riehl, "Physics of ice," (Plemun, New York, 1969) Chap. Protonic conduction of ice: part II: low temperature region, pp. 430–442.
[25] S. Kawada, J. Phys. Soc. Jpn. **44**, 1881 (1978).
[26] C. A. Coulson and D. Eisenberg, Proc. Roy. Soc. London A **291**, 445 (1966).
[27] C.-W. Lee, P.-R. Lee, Y.-K. Kim, and H. Kang, J. Chem. Phys. **127**, 084701 (2007).
[28] H. Gränicher, Phys. Kondens. Materie. **1**, 1 (1963).
[29] A. A. Khamzin and R. R. Nigmatullin, J. Chem. Phys. **147**, 204502 (2017).
[30] D. L. Sidebottom, Rev. Mod. Phys. **81**, 999 (2009).
[31] D. A. Keen and A. L. Goodwin, Nature **521**, 303 (2015).
[32] J.-U. Hoffmann, K. Siemensmeyer, S. Isakov, D. J. P. Morris, B. Klemke, I. Glavatskyi, K. Seiffert, D. A. Tennant, S. Sondhi, and R. Moessner, "Neutron study of the topological flux model of hydrogen ions in water ice," (2018), http://dx.doi.org/10.5442/ND000001.